

A Three-Color, Solid-State, Three-Dimensional Display

Elizabeth Downing,* Lambertus Hesselink, John Ralston, Roger Macfarlane

A three-color, solid-state, volumetric display based on two-step, two-frequency upconversion in rare earth-doped heavy metal fluoride glass is described. The device uses infrared laser beams that intersect inside a transparent volume of active optical material to address red, green, and blue voxels by sequential two-step resonant absorption. Three-dimensional wire-frame images, surface areas, and solids are drawn by scanning the point of intersection of the lasers around inside of the material. The prototype device is driven with laser diodes, uses conventional focusing optics and mechanical scanners, and is bright enough to be seen in ambient room lighting conditions.

The ability to visualize real-time volumetric data in true three-dimensional (3D) form has been a goal of display development efforts for many years. Several clever techniques have been developed, but none has provided a complete solution for the need to view dynamic volumetric data in a realistic interactive format. We present a volumetric display technology that is capable of displaying 3D objects in real time and in true 3D spatial form. The device can be viewed from any perspective, through all sides of the display volume, and does not require special glasses or headgear. The device features unencumbered viewing access to multiple users simultaneously and is capable of displaying information using the three additive primary colors red, green, and blue (Fig. 1).

Background. Three-dimensional perception is a complex cognitive process involving the eyes and the brain as a visual system. Historical solutions to displaying 3D information are diverse and varied and have often relied on tricking the human visual system into thinking that it is seeing a 2D scene in three dimensions. Although specific system requirements vary for different applications, a successful 3D display should provide the viewer, to the necessary extent, with a number of intrinsic visualization parameters. These parameters include the field of view, which is defined by the solid angle subtended by the object and thus determines the apparent size of an

object as seen by the viewer, and the viewing zone, which is defined as the range over which the user or users can move and still clearly see the objects displayed in the field of view. Autostereoscopic viewing is the ability for the displayed objects to be continuously viewable from all regions within the viewing zone, and accommodation is the ability for the user to focus on selected depth planes within the object. Dynamic and real-time capabilities allow moving objects to be displayed at a refresh rate sufficient to avoid flicker (30 to 60 Hz), and interactive capability allows the user to modify the objects being displayed, that is, zoom, translate, rotate, cut, and paste. Color refers to the ability to address three primaries such as the additive red, green, and blue (RGB), from which a wide spectrum of colors, including white, can be produced by appropriate mixing.

Many of the systems that have been developed to date, such as holographic and stereoscopic displays (1), have limited viewing zones and usually present static images or images with very low resolution. Others, like virtual reality displays (2), require the user to wear special headgear that interferes with normal visual processes. Display approaches in which 2D reflective (3) or emissive (4) surfaces are swept throughout a third dimension have been demonstrated, but they too have restricted viewing zones and require large surfaces to be deflected or rotated at high speeds. The traditional 2D cathode-ray tube (CRT) and liquid-crystal displays (LCDs), in which dynamic 3D scenes can be rendered with the use of appropriate graphic constructs such as shading, shadowing, and perspective, have thus far received the highest degree of implementation for the visualization of many types of 3D data. These systems however, display 3D information from only one viewer perspective,

which prevents the user from employing natural human depth cues such as stereo vision and motion parallax. Multiplexing methods that attempt to introduce stereoscopic viewing capabilities into CRT displays have resulted in reduced viewing zones and the need for the user to wear glasses or tracking headgear. None of the approaches that have been presented thus far has provided a complete method for displaying dynamic volumetric data without intrinsic limitations to visualization.

The display concept described in this article has been demonstrated in a small-scale proof-of-principle prototype and provides a solution in which all of these visualization parameters have an attractive range of values. A previous attempt to demonstrate this technique, made by Lewis *et al.* of Battelle Laboratories in the early 1970s (5), succeeded in generating two faint spots of light inside a crystal of erbium-doped calcium fluoride with the use of filtered xenon lamps as excitation sources. The pioneering work of this group of researchers pointed out the potential advantages of such a display and indicated that the shortcomings were primarily associated with the lack of suitable excitation sources and materials with sufficient infrared-to-visible conversion efficiency. We have used high-power laser diodes (6) and improved upconversion materials to lay the critical foundation for this 3D display technology. Of particular importance to the technique are the absorption cross sections and intermediate-level lifetimes of the active ions and the spectral distribution of the fluorescence. Here we describe the fabrication and optimization of upconversion materials and the integration of these materials with laser diodes and scanning systems to create a three-color, solid-state, 3D display.

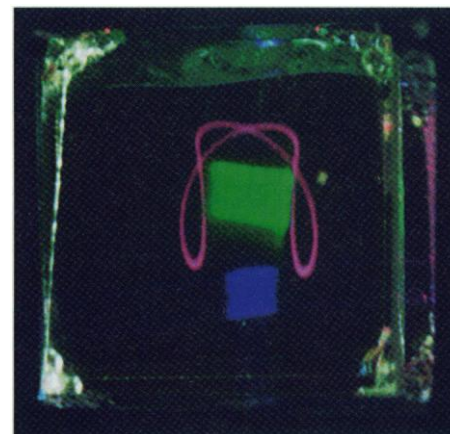


Fig. 1. Taken in ambient room light, this photograph shows a red Lissajous figure and blue and green surface areas that have been drawn, by using IR pump lasers, in our small-scale, prototype solid-state, 3D display.

E. Downing is in the Mechanical Engineering Department, Stanford University, Stanford, CA 94305 and at 3D Technology Laboratories, Post Office Box 114, 200 Blossom Lane, Mountain View, CA 94042, USA. L. Hesselink is in the Electrical Engineering Department, Stanford University, Stanford, CA 94305, USA. J. Ralston is at SDL Corporation, 90 Rose Orchard Way, San Jose, CA 95134, USA. R. Macfarlane is at IBM Almaden Research Center, 650 Harry Road, San Jose, CA 95120, USA.

*To whom correspondence should be addressed. E-mail: 3dlabs@pipeline.com

Principle of operation. The physical mechanism on which this 3D display technology is based is known as two-step, two-frequency (TSTF) upconversion. This phenomenon occurs when an active ion that has been doped in small quantities into a bulk transparent host material is optically excited to higher energy levels by absorbing energy from two different-wavelength, near-infrared (IR) laser beams. The active ion, which normally occupies its lowest energy level E_0 , can absorb energy from the first IR laser beam (wavelength λ_1), making a transition to the intermediate excited state E_1 , where it will stay for the lifetime τ_1 of this level. If the second IR laser beam impinges on this ion while it is in the first excited state, it will absorb energy at the second laser wavelength λ_2 and undergo a transition to the second excited state E_2 . An ion that has been excited in this manner has effectively summed the energy it absorbed from both pump photons and can re-emit most of it as a single photon of visible light by decaying back to the ground state (Fig. 2A).

It is crucial that the two-step excitation process in the active ion occurs from only the selective absorption of two different IR wavelengths, as it is this mechanism that enables a visible point of light to be “turned on” only where the two laser beams cross and nowhere else. By controlling the spatial coordinates of the intersection of the two lasers, one can address a “voxel,” or volumetric pixel, at a specific location inside the bulk imaging medium (Fig. 2B). Rapidly scanning the point of intersection around inside the display volume moves the position of the voxel and allows 3D images to be drawn.

Description of the prototype device. Figure 1 shows a photograph of simple images that have been drawn in our prototype solid-state, 3D display. The photograph was taken in ambient room lighting conditions, and all of the objects drawn in the display were easily visible. Red, green, and blue

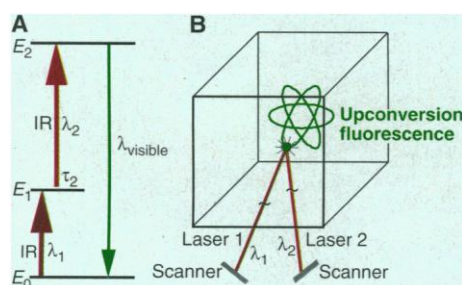


Fig. 2. (A) Energy level diagram of active ion. The display’s principle of operation is based on a phenomenon called TSTF upconversion, which can occur in a specific type of active ion. (B) Two scanned, intersecting laser beams are used to address voxels and draw objects in a transparent material doped with such an ion.

Lissajous figures were created in a stack of three individual glass layers that were laminated together with index-matching optical adhesive to form a composite structure. Each layer was doped with a different ion and was pumped with the wavelength combination appropriate for that dopant. All of the wavelengths required to resonantly pump each of the necessary dipole transitions in these rare earth ions are commercially available as laser diodes at power levels greater than 100 mW (7) (Table 1). Simple mechanical scanners, driven by function generators at rates of 30 to 100 Hz, were used to deflect the laser beams into the 1.5 cm by 1.5 cm by 1.5 cm composite sample. Resolution and voxel size in this display are determined by the diameters of the intersecting laser beams, which when focused to 100- μ m spot sizes produce roughly 300 voxels along the perimeter of a 1.0-cm-diameter circle.

The transparent host materials used for this display are heavy metal fluoride glasses (HMFG) (8) doped with rare earth lanthanides: praseodymium (red), erbium (green), and thulium (blue) (9). These glasses, the most common of which is ZBLAN (10), have been developed for fiber laser and optical amplifier applications (11) and are characterized by low ($<500 \text{ cm}^{-1}$) phonon energies, a critical parameter leading to reduced nonradiative losses and increased upconversion efficiencies. Low-phonon energy glasses offer several distinct advantages over crystalline material hosts. They are relatively easy to manufacture, enabling device performance to be investigated in a wide range of compositions. In addition, they can be easily cast into a variety of shapes from which to construct a display volume. Glasses are isotropic and have no polarization restrictions on pump lasers, assuring that light is emitted isotropically from any voxel. Glasses also introduce inhomogeneous broadening into the electronic transitions of the active ions, creating absorption resonances that are several tens of nanometers wide. Although this feature facilitates pumping with laser di-

odes—as absorption is insensitive to wavelength drift, feedback susceptibility, and astigmatic focusing—it can reduce the absorption cross sections and increase single-frequency upconversion. Glass ceramics (12), which offer the fabrication ease of glasses along with increased absorption cross sections, may provide improved materials for this display technology.

We fabricated various fluoride glasses by melting optical-grade precursor materials in vitreous carbon crucibles under a reactive atmosphere of 3% Cl_2 (balance N_2). Melting temperatures between 700° and 850°C were used, with homogenizing soak cycles ranging from 1.0 to 1.5 hours. Rapid quenching of the molten sample material was accomplished by removing the crucibles from the heat source and introducing convective cooling with dry N_2 gas. Samples on the order of tens of cubic centimeters with no observable crystals under $\times 20$ magnification were routinely prepared.

Upconversion processes. The trivalent rare earth ions are well known for their ability to absorb IR energy and become excited to higher metastable quantum states. Their 4f electronic levels are well shielded from the ligand fields in crystalline and vitreous hosts by the outer 5s and 5p electrons, yielding long-lived metastable lifetimes. Figure 3A shows the energy level diagrams of the lanthanide ions used in our display, along with the pump laser wavelengths and fluorescent emission lines. The $2^{S+1}L_J$ notation used to label the various levels in these ions refers to the spin (S), orbital (L), and total (J) angular momentum quantum numbers of the free ions. Selection rules based on these quantum numbers govern transition probabilities between the atomic levels (13).

A steady-state rate-equation analysis of TSTF excitation, using a simplified five-level model (14) (Fig. 3B), shows how the total power P_v emitted from a single voxel at the intersection of the two resonant pump laser beams depends on the various excitation and material parameters

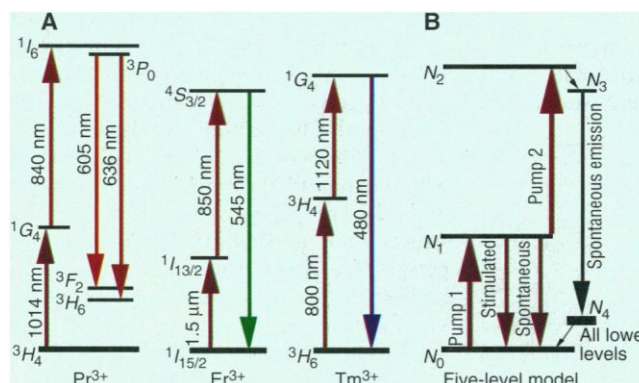


Fig. 3. (A) Energy level diagrams of Pr^{3+} , Er^{3+} , and Tm^{3+} . (B) Five-level rate equation model used to derive Eq. 1. The $2^{S+1}L_J$ notation used to label the levels refers to the spin (S), orbital (L), and total (J) angular momentum quantum numbers of the free ions.

Table 1. Excitation parameters and material properties of prototype three-color, solid-state, 3D display. RE, rare earth.

Color	RE ion	Glass composition	λ_1 (nm)	Laser 1	P_1 (W)	λ_2 (nm)	Laser 2	P_2 (W)	σ_1 (cm ²)	τ_1 (ms)
Red	0.1% Pr ³⁺	ZBLNaCl	1014	SDL #5762 MOPA	1	840	SDL #5430	0.2	2.1×10^{-21}	0.18
Green	0.5% Er ³⁺	ZBLAN	1550	SDL #64-SPE-1550	0.1	850	SDL #5430	0.2	4.5×10^{-20}	15
Blue	0.5% Tm ³⁺	ZBLAN	800	Ti:Al ₂ O ₃	0.4	1064	Nd:YAG	4	1.5×10^{-20}	1.5
			800	SDL #2350*	0.5	1120	SDL #64-SPE-1120*	0.5		

*Available but not used in Fig. 1.

$$P_v = \xi \left(\frac{P_1 P_2}{A^2} \right) \left(\frac{\hbar \omega_{34}}{\hbar \omega_{01} \hbar \omega_{12}} \right) N_T V \sigma_1 \sigma_2 \tau_1 \quad (1)$$

where ξ is the fraction of light emitted in the useful bandwidth, P_1 and P_2 are the powers of the two pump laser beams, A is the area of the focused spot, \hbar is Planck's constant h divided by 2π , ω_{ij} are the transition frequencies between levels i and j , N_T is the dopant concentration, V is the voxel volume, σ_1 and σ_2 are the ground-state and excited-state absorption cross sections, and τ_1 is the lifetime of the intermediate level. The term ξ can be obtained from a calculation of the branching ratios to the different final states. Equation 1 assumes perfect overlap of the two pump lasers. Using a 0.5% ($N_T = 2.5 \times 10^{19} \text{ cm}^{-3}$) erbium-doped HMFG, which has a τ_1 of 15 ms, and σ_1 and σ_2 (15) on the order of 10^{-20} cm^2 , a $100\text{-}\mu\text{m}^3$ voxel can be excited to emit 0.5 μW of total power (the equivalent of that emitted by a single pixel in a high-intensity CRT or LCD display) with about 20 mW of pump power from each laser. This calculation assumes optimum pumping conditions in which the wavelengths of both lasers are resonantly matched to the transition frequencies ω_{ij} of the dopant. Voxel brightness is maximized when the excitation periods are greater than or equal to τ_1 . The lifetime of the intermediate E_1 level should be long enough to allow efficient filling by a continuous-wave laser but short enough to prevent "ghost" voxels from being created at previously scanned locations; the lifetime of the excited E_2 level should be short enough to allow dynamic objects to be drawn without smearing the image. Commercial diode lasers are capable of output powers from hundreds of milliwatts to several watts (7) and can readily provide the pump power needed to implement this technology. Materials with larger absorption cross sections and longer intermediate lifetimes will provide better performance by reducing the power requirements of the display.

Red upconversion fluorescence was induced in Pr³⁺-doped fluoride glass by pumping with 1014 and 840 nm (16) (Fig. 3A). The absorption cross section of the ³H₄ to ¹G₄ transition is small, partly because it is forbidden by spin selection rules. The ¹G₄ level has a lifetime as long as 0.325

ms, depending on the material host and dopant concentration (17). The ¹G₄ to ¹I₆ transition in the Pr³⁺ ion has an absorption cross section that is two orders of magnitude higher than the ground-state cross section (14). Energy absorbed into the ¹I₆ level quickly relaxes to the nearby lower ³P₀ level by nonradiative processes and is emitted predominantly as red light at 605 nm (³P₀ to ³H₆) and 636 nm (³P₀ to ³F₂).

Two-step, two-frequency upconversion fluorescence to green was induced in Er³⁺-doped fluoride glass. All of the relevant transitions in erbium are spin-allowed, yielding high absorption cross sections. The green emission shown in Fig. 1 at 545 nm was induced in an erbium-doped sample with the use of pump wavelengths of 1.5 μm and 850 nm. Erbium-doped materials are also subject to single-frequency upconversion when pumped at 1.5 μm , especially at dopant concentrations greater than a few mole percent. This phenomenon has been used to make single-frequency pumped erbium upconversion lasers (18) but is detrimental to the TSTF absorption processes needed for 3D display applications, as it will make the 1.5- μm pump laser beam itself visible as a green line inside the display volume. Single-frequency upconversion in erbium is a higher order, intensity-dependent process that requires at least three 1.5- μm pump photons to be absorbed to produce one at 545 nm. Scanning the pump laser beams inside the display at a sufficiently high rate decreases the excitation period and reduces single-frequency upconversion in erbium to a magnitude where it is not noticeable to the viewer.

Upconversion fluorescence to blue at 480 nm was induced in Tm³⁺-doped fluoride glass (19). The first transition in thulium (³H₆ to ³H₄) is resonant with 800 nm, and the second step, with 1120 nm. The square, blue surface area in Fig. 1 was pumped with a second-step wavelength of 1064 nm from a Nd:yttrium-aluminum-garnet (YAG) laser. Although the second pump wavelength was more than 60 nm off resonance from the peak absorption frequency of the transition, the TSTF process was still induced in the glass host. Although this example illustrates the advantage of using vitreous materials

when pumping nonresonantly, exactly resonant excitation of this transition will lower the power requirement.

Figure 4 shows the spectral content of the red, green, and blue fluorescence obtained from the TSTF pumping schemes in praseodymium-, erbium-, and thulium-doped fluoride glasses. Although each of these ions also yields some emission at other wavelengths, the primary color components are in the indicated RGB bands, and it is merely fortuitous that the spectral peaks provide three saturated primaries encompassing the human visual color gamut.

Conceptual system architecture. A variety of system architectures can be envisioned in which to implement this solid-state, 3D display concept to provide multiple, individually addressable colors. The three colors shown in Fig. 1 were drawn in materials with dopant concentrations of around 0.5 mol %, a value that has been experimentally determined to maximize voxel brightness. Higher concentrations of the dopants lead to decreased upconversion efficiency because of cross-relaxation between the ions, which depletes the populations of the intermediate levels. This decreased upconversion has, unfortunately, prevented co-doping of all three ions into a single monolithic bulk medium to obtain wavelength-addressable color. The problem of mixing the dopants is compounded by

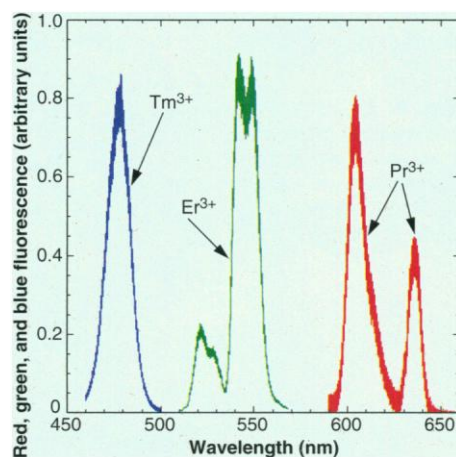


Fig. 4. Spectral content of the red, green, and blue upconversion fluorescence in two-frequency pumped Pr³⁺-, Er³⁺-, and Tm³⁺-doped HMFGs.

the pump wavelengths used to induce TSTF upconversion in one ion inducing single-frequency upconversion in another ion, even at total dopant concentrations below 0.1 mol %. Single-frequency upconversion in other than the target ion causes the IR pump wavelengths to show up as visible lines in the display and causes the spectral content of a single voxel to be composed of emission lines from multiple dopant ions with an overall voxel brightness that is weaker in magnitude.

A better way to achieve a large-scale three-color system may be to implement a composite structure consisting of a repeated sequence of three singly doped layers (20) (Fig. 5). In this configuration, the three individual colors would be addressed in three different thin (100 to 500 μm) material layers, each of which would be optimized with a different dopant and host glass composition. A broad color spectrum, including white, could be created by controlling the intensity ratio of voxels in three adjacent layers, in much the same way as color is created by addressing three closely spaced pixels in a CRT display (21). Layering the display volume provides the added feature of spatially separating the wavelength pairs required to address each color. This is an important consideration as erbium, for example, will undergo single-frequency upconversion when pumped with the excitation wavelengths for thulium and praseodymium. A three-layer stack of individual colors could be repeated over and over again to form the total display volume. This concept offers complete wavelength-addressable RGB capability with one-third the resolution of a monochrome device.

A layered material system also intrinsically incorporates a parallel system architecture into its design. We define η_p , the single-voxel pump efficiency of the material, as the ratio of the total power emitted from a single voxel (P_v) divided by the total power ($P_T = P_1 + P_2$) of the two

input pump lasers. Simple calculations show that the total power required to pump N^3 voxels can be given by $P_T = N^3 P_v / (1/\eta_p)$, or

$$\frac{E_T}{\tau_{ex}} = \frac{N^3 E_v}{\tau_{ex}} \left(\frac{1}{\eta_p} \right) \quad (2)$$

where E_T is the pump energy, E_v is the energy emitted by the voxel, and τ_{ex} is the excitation period. Equation 2 shows that a voxel need not emit light continuously but can be excited to emit a higher amount of energy for a shorter period of time ($P_v = E_v/\tau_{ex}$) if it is pumped strongly and refreshed again a short time later. A single voxel ($N = 1$) that is pumped with 30 times the excitation energy for 1/30th of a second ($P_T = E_T/\tau_{ex}$) and refreshed once a second will emit the same average power as one that is pumped continuously at P_T . In order to address N^3 voxels every 1/30th of a second using only two lasers, the scan rate must be $N^3 \times 30$ Hz. A 3-MHz scan rate would be needed to address 100,000 voxels, producing an excitation period of 0.3 μs per voxel ($R_S = 1/\tau_{ex}$) and requiring a pump energy 100,000 times greater than that necessary to turn on a single voxel at 30 Hz. A pump energy this high would be above the damage threshold of most optical materials. The inadequacy of using only two pump lasers arises because only a small portion of the available power along each beam ($\sim 100 \mu\text{m}$) can be used at any particular instant to excite a voxel, leaving the remaining length of each beam unused. The overall efficiency of this system can therefore never be greater than the single-voxel pump efficiency of the material, η_p . If, on the other hand, a system design using parallel pump lasers to simultaneously excite multiple voxels along the length of each beam is used, more of the available power in the lasers could be utilized, reducing scan speeds and data rates of the system. For example, two orthogonal, linear laser diode arrays with 100 emitters each can

address 10,000 voxels in a plane when turned on simultaneously (Fig. 6). This yields a device efficiency equal to $100\eta_p$ ($100P_1 + 100P_2 = 10,000 P_v$) or two orders of magnitude greater than a two-laser system pumping 10,000 voxels. Lowering the power of the lasers is also attractive from a safety standpoint because any pump power that is not absorbed by the active medium requires filtering at the viewing surface of the display. Parallel system architecture, combined with appropriate multiplexing algorithms, could increase the device efficiency of the display beyond the single-voxel pump efficiency of the material by allowing for more effective use of available pump power.

Monochrome systems in which only one color need be addressed (Fig. 7) would require only one dopant ion in the display medium and could be implemented with a similar parallel excitation architecture. The display volume could be either monolithic or constructed compositely from layers or blocks of material, which could be substantially thicker than the layers needed for a color display. These layers could vary in dopant concentration, with higher doped layers placed farther away from the laser pump sources, producing an absorption gradient. This design could be used to balance the reduction in pump power that occurs as the ground-state laser beam propagates through the material and is absorbed. A

Fig. 5. Layered device architecture proposed for providing wavelength-addressable red, green, and blue colors in a solid-state, 3D display.

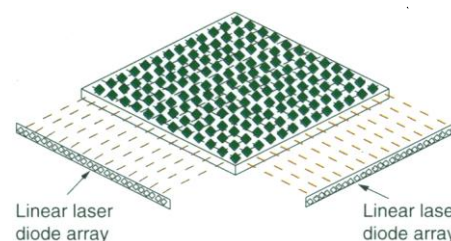
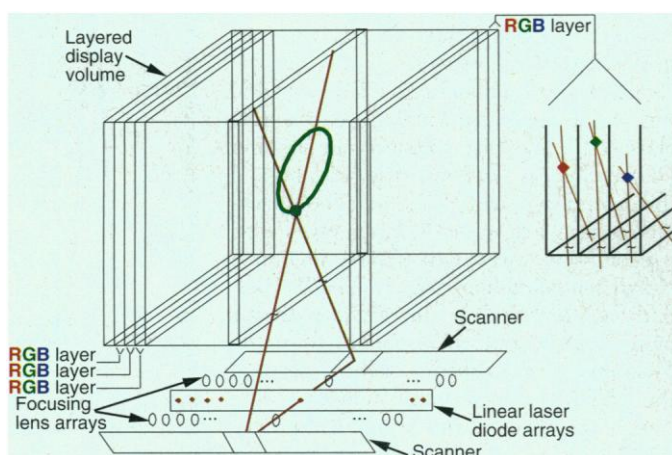


Fig. 6. Illustration of how parallel architecture can improve device performance above the single-voxel pump efficiency of the material, η_p , by addressing N^2 voxels with $2N$ lasers.

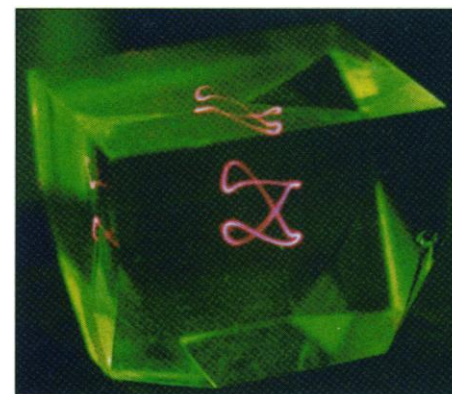


Fig. 7. Photograph of a monochrome, solid-state, 3D display in a 1-cm³ Pr³⁺-doped sample.

layered structure would also help to reduce some of the practical issues associated with casting a large monolithic piece of low-phonon energy glass, as these materials have a low thermal conductivity and are difficult to fabricate in pieces thicker than a few inches. Such a structure would enable large displays having several inches on a side to be manufactured.

Conclusion. The solid-state, 3D display technology described here can be driven entirely with commercially available laser diodes and scanning systems and can be powered directly from 120-V, 60-Hz electrical outlets. The display operates at room temperature and is viewable under typical ambient room lighting conditions. Current efforts are under way to implement a more fully integrated system architecture and to increase upconversion efficiencies with improved material systems. We believe that this technique offers a viable approach for presenting real-time, multidimensional information to a multitude of viewers, independent of viewing perspective, with no obstructed viewing regions and no need for special viewing eyewear.

REFERENCES AND NOTES

1. P. St. Hilaire, *Opt. Eng.* **34**, 83 (1995).
2. S. Bryson, *Proc. SPIE* **1915**, 155 (1993).
3. P. Soltan, J. Trias, W. Robinson, W. Dahlke, *ibid.* **1664**, 177 (1992).
4. D. G. Jansson and R. P. Kowsowsky, *ibid.* **507**, 82 (1984).
5. J. D. Lewis, C. M. Verber, R. B. McGhee, *IEEE Trans. Electron Devices* **18**, 724 (1971).
6. D. F. Welch, in *14th IEEE International Semiconductor Laser Conference* (IEEE, New York, 1994), pp. 3-5.
7. SDL Corporation, *1996 Product Catalog* (San Jose, CA, 1996).
8. I. D. Aggarwal and G. Lu, Eds., *Fluoride Glass Fiber Optics* (Academic Press, New York, 1991).
9. G. H. Dieke and H. M. Crosswhite, *Appl. Opt.* **2**, 675 (1963).
10. M. Robinson, R. C. Pastor, R. R. Turk, M. Braunstein, R. Braunstein, *Mater. Res. Bull.* **15**, 735 (1980).
11. M. J. F. Digonnet, Ed., *Rare-Earth-Doped Fiber Laser Sources and Amplifiers* (SPIE Optical Engineering Press, Bellingham, WA, 1992).
12. P. A. Tick, N. F. Borrelli, L. K. Cornelius, M. A. Newhouse, *J. Appl. Phys.* **78**, 6367 (1995).
13. C. Cohen-Tannoudji, B. Diu, F. Laloë, *Quantum Mechanics* (Wiley, New York, 1977).
14. A. C. Tropper *et al.*, *J. Opt. Soc. Am. B* **11**, 866 (1994).
15. R. S. Quimby and B. Zheng, *Mater. Res. Soc. Symp. Proc.* **244**, 169 (1992).
16. R. G. Smart *et al.*, *Electron. Lett.* **27**, 1307 (1991); E. A. Downing, L. Hesselink, R. M. Macfarlane, *International Display Research Conference*, Monterey, CA, 10 to 13 October 1994, p. 321.
17. M. A. Newhouse, R. F. Bartholomew, B. G. Aitken, L. J. Button, N. F. Borrelli, *IEEE Photonics Technol. Lett.* **6**, 189 (1994).
18. R. M. Macfarlane, E. A. Whittaker, W. Lenth, *Electron. Lett.* **28**, 2136 (1992).
19. E. A. Downing, L. Hesselink, R. M. Macfarlane, *Proc. IEEE Nonlinear Optics: Materials, Fundamentals, and Applications* (Optical Society of America, Washington, DC, 1994), p. 409.
20. J. T. Veligdan, *Proc. SPIE* **2462**, 94 (1995).
21. A. M. Morrell, *Proc. SID* **22**, 3 (1981).
22. We acknowledge R. Klein and D. Evans of SDL for their valued technical assistance with laser diodes,

and N. Borrelli and R. Bartholomew of Corning for performing lifetime measurements. We also acknowledge R. Fogelson of Stanford's Center for Materials Research for the use of facilities and equipment. E.D. personally thanks J. Trias and P. Soltan of Naval Research and Development, two visionaries who believed in her enough to fund this research at

Stanford 3 years ago under contract N6600-92-D-0092. This work was also supported in part by L. N. Durvasula of the Advanced Research Projects Agency under contract N0014-92-J-1903 through the Stanford Center for Nonlinear Optical Materials.

14 March 1996; accepted 11 July 1996

RNA Editing: A Mechanism for gRNA-Specified Uridylate Insertion into Precursor mRNA

Moffett L. Kable,* Scott D. Seiwert,* Stefan Heidmann, Kenneth Stuart†

In the mitochondria of trypanosomatid protozoa the precursors of messenger RNAs (pre-mRNAs) have their coding information remodeled by the site-specific insertion and deletion of uridylate (U) residues. Small trans-acting guide RNAs (gRNAs) supply the genetic information for this RNA editing. An in vitro system was developed to study the mechanism of U insertion into pre-mRNA. U-insertion editing occurs through a series of enzymatic steps that begin with gRNA-directed pre-mRNA cleavage. Inserted U's are derived from free uridine triphosphate and are added to the 3' terminus of a 5' pre-mRNA cleavage product. gRNA specifies edited RNA sequence at the subsequent ligation step by base pairing-mediated juxtaposition of the 3' cleavage product and the processed 5' cleavage product. gRNA/pre-mRNA chimeras, purported intermediates, seem to be abortive end products of the same reaction.

Most mitochondrial pre-mRNAs in trypanosomes undergo RNA editing, a form of RNA processing that markedly alters their U content and consequently changes their coding information (1). In *Trypanosoma brucei*, RNA editing inserts a total of 3030 U's into hundreds of editing sites in 12 different pre-mRNAs. RNA editing also removes U's from specific positions, but at a 10-fold lower frequency. Both types of changes in informational content are specified by small [~ 60 nucleotides (nt)], trans-acting RNAs termed gRNAs. The mitochondrion of *T. brucei* contains numerous gRNAs, each of which is complementary to a region of an edited mRNA and which collectively are diverse enough in sequence to specify all of the observed editing.

The exact mechanistic role of gRNAs in RNA editing is not well defined. Before U insertion and deletion, the 5' portion of a gRNA is thought to form a short intermolecular duplex with its cognate pre-mRNA immediately 3' of the region to be processed. Mismatched purines in the gRNA sequence

adjacent to this duplex then specify U insertion, whereas mismatched U's in the adjacent pre-mRNA sequence are deleted. Both events extend the complementarity between gRNA and pre-mRNA to produce an uninterrupted intermolecular helix.

Elucidation of the biochemical mechanism of RNA editing and its component steps hinges on identifying the source of inserted U's. In alternative models of RNA editing, either free uridine triphosphate (UTP) (2) or nonenclosed U residues at the 3' end of gRNAs (3) have been suggested as the source of these residues.

We have developed a cell-free system that reproduces U-insertion editing in vitro and which therefore allows direct analysis of the mechanism of this reaction. (The insertion or deletion of U's at one editing site is referred to as the editing "reaction," although it occurs by a series of catalytic steps.) We compare this mechanism to that of the less frequent U-deletion editing previously examined (4).

U insertion is gRNA- and UTP-dependent. To study U insertion, we used a synthetic transcript based on adenosine triphosphatase 6 pre-mRNA (A6-eES1) (Fig. 1) (5) as an editing substrate. It corresponds to an RNA that is edited at only the 3'-most editing site (ES1) by the deletion of two U's. The gRNA termed gA6[14] (6) is predicted to direct the insertion of

M. L. Kable and K. Stuart, Seattle Biomedical Research Institute, Seattle, WA 98109, and Department of Pathobiology, University of Washington, Seattle, WA 98195, USA.

S. D. Seiwert and S. Heidmann, Seattle Biomedical Research Institute, Seattle, WA 98109, USA.

*These authors contributed equally to this work.

†To whom correspondence should be addressed. E-mail: kstuart@u.washington.edu